







Rician Noise Estimation for 3D Magnetic Resonance Images Based on Benford's Law

Rosa Maza-Quiroga^{1,3} , Karl Thurnhofer-Hemsi^{1,3} ,
Domingo López-Rodríguez^{2,3} , and Ezequiel López-Rubio^{1,3} 

¹ Department of Computer Languages and Computer Science,
Universidad de Málaga, Málaga, Spain

{rosammq,karkhader,ezeqlr}@lcc.uma.es, dominlopez@uma.es

² Department of Applied Mathematics, Universidad de Málaga,
Bulevar Louis Pasteur, 35, 29071 Málaga, Spain

³ Biomedic Research Institute of Málaga (IBIMA), Málaga, Spain

Abstract. In this paper, a novel method to estimate the level of Rician noise in magnetic resonance images is presented. We hypothesize that noiseless images follow Benford's law, that is, the probability distribution of the first digit of the image values is logarithmic. We show that this is true when we consider the raw acquired image in the frequency domain. Two measures are then used to quantify the (dis)similarity between the actual distribution of the first digits and the more theoretical Benford's law: the Bhattacharyya coefficient and the Kullback-Leibler divergence. By means of these measures, we show that the amount of noise directly affects the distribution of the first digits, thereby making it deviate from Benford's law. In addition, in this work, these findings are used to design a method to estimate the amount of Rician noise in an image. The utilization of supervised machine learning techniques (linear regression, polynomial regression, and random forest) allows predicting the parameters of the Rician noise distribution using the dissimilarity between the measured distribution and Benford's law as the input variable for the regression. In our experiments, testing over magnetic resonance images of 75 individuals from four different repositories, we empirically show that these techniques are able to precisely estimate the noise level present in the test T1 images.

Keywords: MRI · Rician noise · Benford's law · Noise estimation

1 Introduction

Real-world magnetic resonance imaging (MRI) data is very often corrupted by a noise component, generated in the acquisition process. The noise is a challenging problem since it degrades the reliability of both radiologists and automatic

computer-aided diagnosis. It also can affect the efficiency of automated quantitative post-processing methods, which are increasingly used nowadays, both in clinical practice and in research.

Denoising methods are an important part of the pre-processing of MRIs, and try to improve the image quality by increasing the Signal-to-Noise Ratio (SNR) while preserving the image features. Currently, many different denoising methods have appeared in the literature. We can find methods based, for example, on the wavelet transform [24], the anisotropic diffusion filter [12] or non-local filters [25], the linear minimum square error [6], a sparse representation learning [3], the singular value decomposition [27] or the maximum likelihood approach [19].

With the rise of deep learning, new denoising techniques have appeared, e.g., the stacked sparse auto-encoder [4], multi-layer perceptron [13] or convolutional neural networks [23]. Using residual learning, the authors in [26] developed a deep denoising convolutional neural network for Gaussian denoising, achieving good performance. Also, in [8], a convolutional neural network is presented for medical image denoising. More recently, attention-guided models such as [22] have been presented, showing good performance.

It is already known that MRI noise follows a Rician distribution [7] and that there is around 60% underestimation of the true noise if the noise in MRI is assumed to be Gaussian. Note that the Rician distribution is signal-dependent, differently from the additive Gaussian noise. Thus, separating noise from the raw MRI without losing critical image features remains a challenging task.

Some of the different denoising algorithms assume that the deviation parameter σ of the Rician distribution which generates the noise is known. Noise parameters can be estimated by using methods based on principal components analysis [15] and on the wavelet transform [2]. The method based on PCA is best suited for weak texture images but not so good for Rician noise estimation. In the wavelet approach, the image is decomposed in sub-bands, of which the HH sub-band is composed of the wavelet noise coefficient. The median of these coefficients is used to compute the *median absolute deviation* estimator for σ . Although this wavelet model fits better Gaussian noise, it can be adequately modified [11] to estimate the σ parameter in Rician noise.

In this work, we propose an alternate technique to estimate the noise deviation parameter, based on Benford's law, that is, in the statistical distribution of the first significant digits in a dataset. Although it is well known that image histogram does not follow Benford's law, certain transformations in the image are consistent with such distribution. Particularly, in [9], it is shown that the gradient and Laplace transform magnitude follows Benford's law, even in medical images such as MRI [20]. Other transformations whose coefficients follow Benford's law are the discrete cosine and wavelet transforms [1].

Our proposal aims at demonstrating that the coefficients of the Fourier transform of an image follow closely Benford's law, and we hypothesize that larger amounts of noise in an image make these coefficients deviate from such distribution. Hence, the level of agreement between the expected distribution and the actual first digit distribution in the Fourier domain is an indicator of the

noise parameter σ . As an application of these results, we show how regression techniques are able to accurately predict the noise level of an image.

2 Methodology

In this section, the proposed methodology to estimate Rician noise in 3D MRIs is presented. It is well known that the noise in magnitude MRIs can be modeled by Rician noise [7]. Let \hat{x} be the original (noiseless) image pixel intensity, and x the measured pixel intensity in the presence of Rician noise of level σ , where σ is the standard deviation of the Gaussian noise affecting the real and imaginary MRIs, so that the Gaussian noise level σ in both real and imaginary images is assumed to be the same. Then the probability distribution for x is given by:

$$p(x) = \frac{x}{\sigma^2} \exp\left(-\frac{x^2 + \hat{x}^2}{2\sigma^2}\right) I_0\left(\frac{x\hat{x}}{\sigma^2}\right) \quad (1)$$

where I_0 is the modified zeroth order Bessel function of the first kind.

In this work we propose to employ Benford's law to estimate the Rician noise level σ . Benford's law is an empirical law which states that the probability distribution $Q(n)$ of the first digit n of the decimal representation of a nonzero real number y is logarithmic [5]:

$$Q(n) = \log_{10}\left(1 + \frac{1}{n}\right), \quad \text{where } n = \left\lfloor \frac{|y|}{10^{\lfloor \log_{10}|y| \rfloor}} \right\rfloor \quad (2)$$

where $n \in \{1, 2, \dots, 9\}$, $|\cdot|$ stands for the absolute value of a real number, and $\lfloor \cdot \rfloor$ denotes rounding towards $-\infty$.

Despite its counter intuitive nature, Benford's law has been found to hold for many datasets coming from natural processes, such as natural images in a transformed domain [1]. Our hypothesis is that the higher the Rician noise corrupting a MRI, the farther that the image departs from Benford's law. This effect is better observed for the values of the 3D Fast Fourier Transform (FFT) of the MRI rather than the raw pixel intensity values because the distribution of the first digits of the latter is affected by the measurable pixel intensity range, while the former is relatively independent from the pixel intensity range. As seen in [21], distributions that have a large width, i.e. they spread their probability mass across several orders of magnitude, follow Benford's law more closely. The raw pixel intensity values have a limited range, so their distribution has a reduced width. On the contrary, the FFT of the raw values is not constrained by this limitation. In fact, the compression/expansion property of the FFT means that the narrower the range of the raw pixel values, the wider the range of their FFT.

Let us note y the 3D FFT of the measured pixel intensity values x , so that the first digit of the decimal representation of y is noted n , as given by (2). Then a measure \mathcal{D} of the dissimilarity of the observed distribution $P(n)$ with respect to Benford's law distribution $Q(n)$ given by (2) must be selected. We

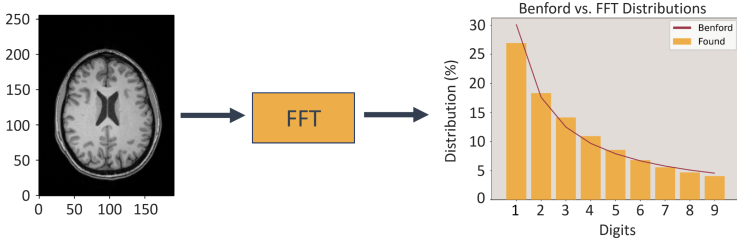


Fig. 1. First step: FFT histogram computation and comparison with Benford’s law.

consider two such measures, namely the Bhattacharyya Coefficient (BC) and the Kullback-Leibler (KL) divergence:

$$\mathcal{D}_{BC} = \sum_{n=1}^9 \sqrt{P(n)Q(n)}, \quad \mathcal{D}_{KL} = \sum_{n=1}^9 P(n) \log \frac{P(n)}{Q(n)} \tag{3}$$

It must be noted that the lower \mathcal{D}_{KL} , the closer the observed distribution $P(n)$ to Benford’s law distribution $Q(n)$. In contrast to this, the higher \mathcal{D}_{BC} , the closer the observed distribution $P(n)$ to Benford’s law distribution $Q(n)$.

After this, the Rician noise level σ of the MRI is estimated as a function of the selected measure \mathcal{D} :

$$\sigma \approx f(\mathcal{D}) \tag{4}$$

where f is estimated by machine learning regression techniques.

3 Experimental Setting

Three types of experiments are presented. First of all, we verify the distribution of the first digit of voxels values of a 3D MRI in the frequency domain resembles Benford’s law. Secondly, we check if the noise in an image disturbs Benford’s law probability distribution. Finally, we propose three types of models to predict the quantity of noise in an MRI.

A total of 75 T1-weighted brain MRIs were selected, being publicly accessible with a non-restrictive license available in Mindboogle [10], from healthy participants, and of high quality to ensure right noise analysis. The images in NIfTI format come from 4 repositories: 12 from HLN [17] with dimension $256 \times 256 \times 170$, 21 from MMRR [14] with dimension $170 \times 256 \times 256$, 20 from NKI-RS [18] and 20 from NKI-TRT [18] with dimension $192 \times 256 \times 256$.

Using all the MRI voxels, the FFT is computed and the probability distribution of each voxel’s frequency of the first digit is constructed. Finally, all the images in the Fourier domain are assessed to follow a distribution that matches Benford’s law. Then, for each image, 20 new images with noised values were generated varying the distortion in the range $[0, 10)$ percent of Rician noise with respect to the amplitude of the signal, following a uniform continuous distribution. Thus, for each repository, we have a new image data set. As explained

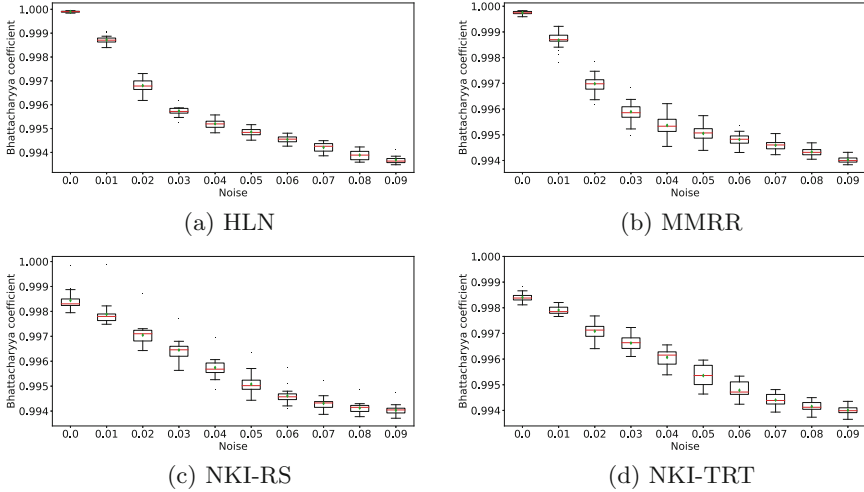


Fig. 2. Evolution of Bhattacharyya coefficient as noise increases in four image repositories. Average is in green diamond and median in red line. (Color figure online)

in Sect. 2, two methods are used to measure the similarity with Benford’s law: BC, belonging to the range $[0, 1]$, where it will be 0 if there is no overlap and 1 if it matches perfectly; and KL divergence, where 0 indicates that the two distributions in question are identical. Since Benford’s law appears to be a noise detector, three types of regressors were used to predict the noise in an image: Linear Regression (LR), Polynomial Regression of degree two (PR) and, Random Forest (RF). The data were split into training (80%) and testing (20%) samples selected from each dataset to validate the considered models.

In order to assess the accuracy of the estimation (4), the Mean Squared Error is employed. In addition, the regression score function, also known as the coefficient of determination, was used to measure the goodness of fit:

$$MSE = \frac{1}{M} \sum_{i=1}^M (\sigma_i - f(\mathcal{D}_i))^2, \quad R^2 = 1 - \frac{\sigma_r^2}{\sigma^2} \quad (5)$$

where M is the total number of test images, σ is the variance of the dependent variable, and the residual variance is σ_r .

In this work, a PC with Intel Core 7 CPU, 32 GB RAM, a NVIDIA TRX2080 Super Ventus, and 1 TB of SSD was used, running under Ubuntu 20.04, and using Python 3.8. The scientific libraries *matplotlib*, *nibabel*, *scipy*, *sklearn*, and *benford* [16] were used. All models were trained using default parameters¹.

¹ The source code with scripts and sample data is available in: https://github.com/icai-uma/RicianNoiseEst_3DMRI_BenfordLaw.git.

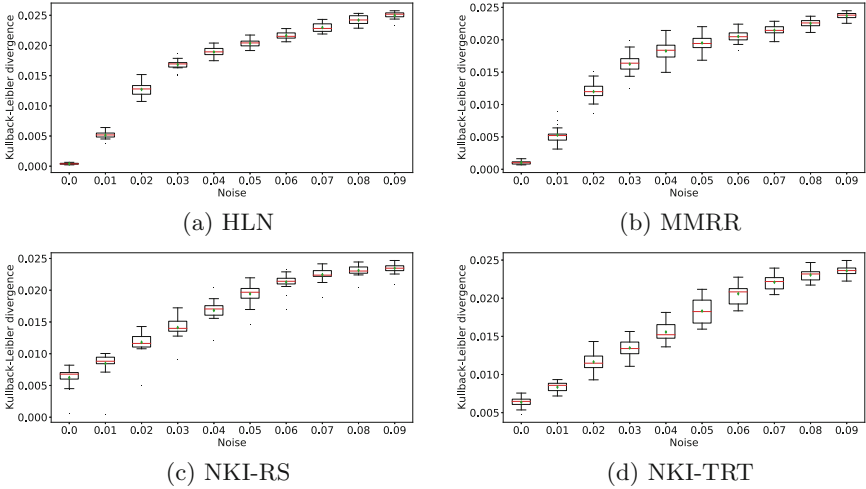


Fig. 3. Evolution of Kullback-Leibler divergence as noise increases in four image repositories. Average is in green diamond and median in red line. (Color figure online)

4 Results

The high quality of the original datasets ensures the right surface reconstruction without noise, and the evidence is shown in Figs.2 and 3. When no noise is added, i.e. 0.0, BC takes values close to 1 and KL values close to 0, especially in HLN and MMRR. The values of BC and KL in NKI-RS and NKI-TRT might be due to the lack of enough quality in the acquisition protocol since BC is between 0.998 and 0.999, and KL is not so close to 0.005. Nevertheless, for all repositories, the overall trend remains presenting very good values of BC and KL without noise. Thus, we accept that a noiseless MRI in the Fourier frequency domain follows Benford’s law.

Table 1. *MSE* and *R*² results of the prediction models by using the Bhattacharyya Distance and Kullback-Leibler divergence for all datasets. *MSE* is multiplied by 10⁻⁵

Metric	Bhattacharyya coefficient						Kullback-Leibler					
	LR		PR		RF		LR		PR		RF	
Dataset	<i>MSE</i>	<i>R</i> ²	<i>MSE</i>	<i>R</i> ²	<i>MSE</i>	<i>R</i> ²	<i>MSE</i>	<i>R</i> ²	<i>MSE</i>	<i>R</i> ²	<i>MSE</i>	<i>R</i> ²
HLN	11.94	0.82	1.87	0.97	2.57	0.96	11.79	0.82	1.83	0.97	2.62	0.96
MMRR	16.93	0.81	5.37	0.94	6.98	0.92	16.58	0.82	5.039	0.94	5.39	0.94
NKI-RS	7.92	0.89	5.76	0.92	6.98	0.91	8.25	0.88	6.09	0.92	8.42	0.89
NKI-TRT	4.98	0.94	4.18	0.95	6.02	0.93	5.15	0.94	4.33	0.95	5.54	0.93

With the addition of noise in the image, the results shown in Figs.2 and 3 indicate that the first digit distribution of an image changes. A dependency

between noise and the parameter’s value is clearly appreciated. The more noise is introduced into the image, the farther the distribution is from Benford’s law. NKI-RS and NKI-TRT present a nearly linear decrease trend in BC and an approximately linear growth trend in KL. On the contrary, the HLN and MMRR repositories show a fast decrease in BC and a rapid KL increase. NKI-TRT boxes are the most extensive compared to other repositories showing a more considerable distance between quantiles, but NKI-TRT has no outliers.

Now, the results of estimating the noise level by means of the regression techniques mentioned above are presented. Note that BC and KL measures have a significance in the order of 10^{-3} . The results of MSE presented in Table 1 are in the order of 10^{-5} , indicating good results with two orders of magnitude lower of the parameters. Besides, in the same table, the R^2 shows values close to 1 in general, so the models fit the data well globally. The best results are generated by PR and followed by RF, and finally LR. The worst results are obtained using LR for MMRR repository and the best are for the PR model with HLN. Models and training data are represented in Figs. 4 and 5. The models fit the training data well without losing test accuracy. As more noise is added, the BC and KL values have a wider range.

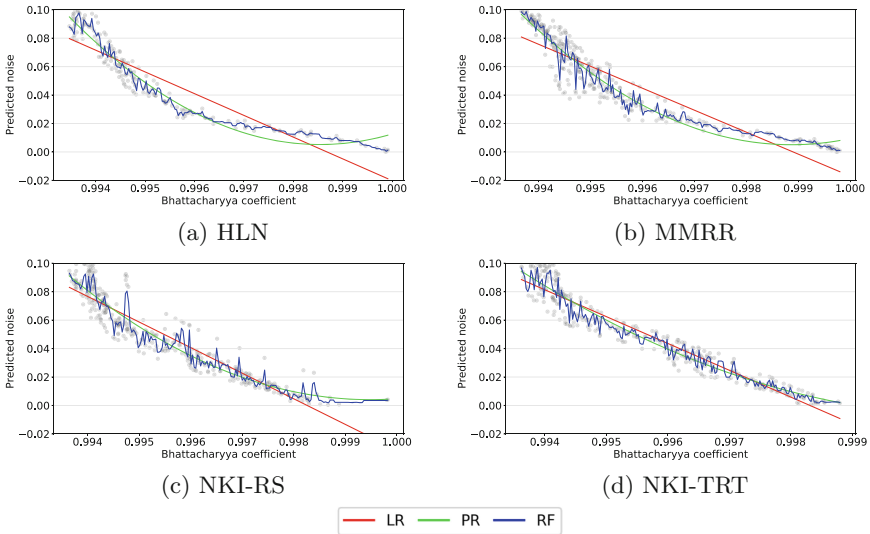


Fig. 4. Bhattacharyya Coefficient training data (black dots) are displayed along with the three models (LR in red, PR in green and RF in blue) in four repositories. (Color figure online)

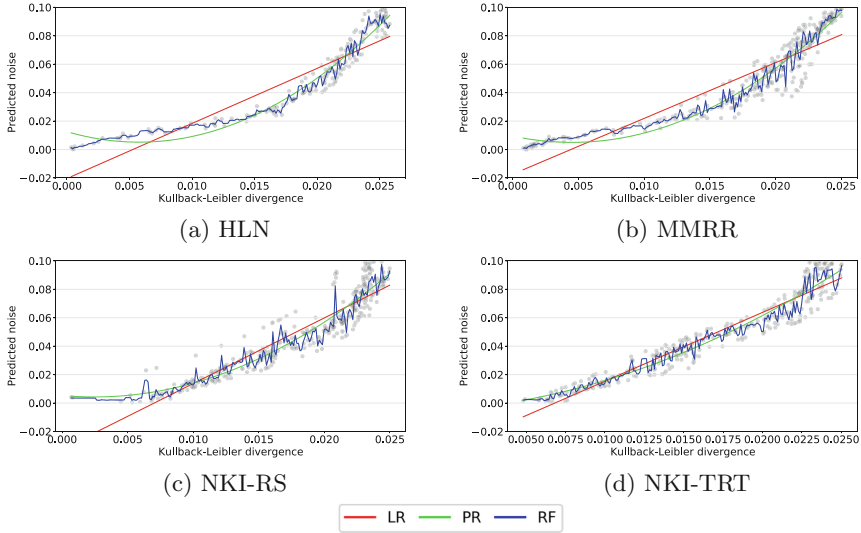


Fig. 5. Kullback-Leibler divergence training data (blue dots) are displayed along with the three models (LR in red, PR in blue and RF in green) in four repositories. (Color figure online)

5 Conclusions

In this work, we have shown that the coefficients of the Fourier transform of a T1 MRI follow Benford’s law, that is, their first digit distribution is logarithmic. We also demonstrate that the amount of Rician noise present in an image directly affects the first digit distribution of the Fourier transform of a T1 MRI, making it deviate from Benford’s law. Hence, by measuring the level of agreement of the distribution of the first digits of the Fourier coefficients with Benford’s law, using the the Bhattacharyya coefficient and the Kullback-Leibler divergence, one can estimate the noise level in a T1 MRI.

In addition, in this paper we show that supervised learning techniques allow estimating the noise level, using the distribution dissimilarity measures mentioned above as regressors. Although not all the datasets have a optimal quality, our experiments over MRIs of 75 individuals confirm that Benford’s law is fulfilled by the Fourier coefficients of noiseless T1 MRIs and that it can be properly used to precisely estimate the noise level, since all the error measures followed a similar tendency. Therefore, further works on denoising algorithms could integrate this methodology to estimate the level of noise. This will make the algorithms work better and have a direct implication in improving radiologists’ diagnoses.

To sum up, our work presents an empirical demonstration of the proposed hypothesis of Benford’s law in the frequency domain and its novel use as a noise estimator with the help of machine learning, providing very promising results.

It must be highlighted that more than one image quality metrics (IQMs) may be required to faithfully evaluate the noise level of an image. Therefore, our proposal is a significant achievement in the search for reliable IQMs.

Acknowledgements. This work is partially supported by the following Spanish grants: TIN2016-75097-P, PIT.UMA.B1.2017, RTI2018-094645-B-I00 and UMA18-FEDERJA-084. All of them include funds from the European Regional Development Fund (ERDF). The authors thankfully acknowledge the computer resources, technical expertise and assistance provided by the SCBI (Supercomputing and Bioinformatics) center of the University of Málaga. They also gratefully acknowledge the support of NVIDIA Corporation with the donation of two Titan X GPUs. The authors acknowledge the funding from the Universidad de Málaga. Rosa Maza-Quiroga is funded by a Ph.D. grant from the Instituto de Salud Carlos III (ISCIII) of Spain under the i-PFIS program (IFI19/00009). Karl Thurnhofer-Hemsi is funded by a Ph.D. scholarship from the Spanish Ministry of Education, Culture and Sport under the FPU program (FPU15/06512).

References

1. Al-Bandawi, H., Deng, G.: Classification of image distortion based on the generalized Benford's law. *Multimedia Tools Appl.* **78**, 25611–25628 (2019)
2. Chang, S.G., Yu, B., Vetterli, M.: Spatially adaptive wavelet thresholding with context modeling for image denoising. *IEEE Trans. Image Process.* **9**(9), 1522–1531 (2000)
3. Chen, W., You, J., Chen, B., Pan, B., Li, L., Pomeroy, M., Liang, Z.: A sparse representation and dictionary learning based algorithm for image restoration in the presence of rician noise. *Neurocomputing* **286**, 130–140 (2018)
4. Dolz, J., et al.: Stacking denoising auto-encoders in a deep network to segment the brainstem on mri in brain cancer patients: a clinical study. *Comput. Med. Imaging Graph.* **52**, 8–18 (2016)
5. Fu, D., Shi, Y.Q., Su, W.: A generalized Benford's law for JPEG coefficients and its applications in image forensics. In: III, E.J.D., Wong, P.W. (eds.) *Security, Steganography, and Watermarking of Multimedia Contents IX*, vol. 6505, pp. 574–584. International Society for Optics and Photonics, SPIE (2007)
6. Golshan, H.M., Hasanzadeh, R.P., Yousefzadeh, S.C.: An mri denoising method using image data redundancy and local snr estimation. *Magn. Reson. Imaging* **31**(7), 1206–1217 (2013)
7. Gudbjartsson, H., Patz, S.: The Rician distribution of noisy MRI data. *Magn. Reson. Med.* **34**(6), 910–914 (1995)
8. Jifara, W., Jiang, F., Rho, S., Cheng, M., Liu, S.: Medical image denoising using convolutional neural network: a residual learning approach. *J. Supercomput.* **75**(2), 704–718 (2019)
9. Jolion, J.M.: Images and benford's law. *J. Math. Imaging Vis.* **14**(1), 73–81 (2001)
10. Klein, A., Tourville, J.: 101 labeled brain images and a consistent human cortical labeling protocol. *Front. Neurosci.* **6**, 171 (2012). <https://doi.org/10.3389/fnins.2012.00171>
11. Koay, C.G., Basser, P.J.: Analytically exact correction scheme for signal extraction from noisy magnitude MR signals. *J. Magn. Reson.* **179**(2), 317–322 (2006)

12. Krissian, K., Aja-Fernández, S.: Noise-driven anisotropic diffusion filtering of MRI. *IEEE Trans. Image Process.* **18**(10), 2265–2274 (2009)
13. Kwon, K., Kim, D., Park, H.: A parallel mr imaging method using multilayer perceptron. *Med. Phys.* **44**(12), 6209–6224 (2017)
14. Landman, B.A., et al.: Multi-parametric neuroimaging reproducibility: a 3-T resource study. *Neuroimage* **54**(4), 2854–2866 (2011). <https://doi.org/10.1016/j.neuroimage.2010.11.047>
15. Liu, X., Tanaka, M., Okutomi, M.: Noise level estimation using weak textured patches of a single noisy image. In: 2012 19th IEEE International Conference on Image Processing, pp. 665–668. IEEE (2012)
16. Marcel, M.: Benford_py: a Python Implementation of Benford's Law Tests (2017). https://github.com/milcent/benford_py
17. Morgan, V.L., Mishra, A., Newton, A.T., Gore, J.C., Ding, Z.: Integrating functional and diffusion magnetic resonance imaging for analysis of structure-function relationship in the human language network. *PLOS ONE* **4**(8), 1–8 (2009). <https://doi.org/10.1371/journal.pone.0006660>
18. Nooner, K.B., et al.: The NKI-Rockland sample: a model for accelerating the pace of discovery science in psychiatry. *Front. Neurosci.* **6**, 152 (2012). <https://doi.org/10.3389/fnins.2012.00152>
19. Rajan, J., Jeurissen, B., Verhoye, M., Van Audekerke, J., Sijbers, J.: Maximum likelihood estimation-based denoising of magnetic resonance images using restricted local neighborhoods. *Phys. Med. Biol.* **56**(16), 5221 (2011)
20. Sanches, J., Marques, J.S.: Image Reconstruction using the Benford Law. In: 2006 International Conference on Image Processing, pp. 2029–2032 (2006). <https://doi.org/10.1109/ICIP.2006.312845>
21. Smith, S.W.: *The Scientist & Engineer's Guide to Digital Signal Processing*. California Technical Publishing, San Diego, CA (1997)
22. Tian, C., Xu, Y., Li, Z., Zuo, W., Fei, L., Liu, H.: Attention-guided CNN for image denoising. *Neural Netw.* **124**, 117–129 (2020)
23. Tripathi, P.C., Bag, S.: Cnn-dmri: a convolutional neural network for denoising of magnetic resonance images. *Pattern Recogn. Lett.* **135**, 57–63 (2020)
24. Yang, X., Fei, B.: A wavelet multiscale denoising algorithm for magnetic resonance (MR) images. *Measure. Sci. Technol.* **22**(2), 025803 (2011)
25. Yu, H., Ding, M., Zhang, X.: Laplacian eigenmaps network-based nonlocal means method for MR image denoising. *Sensors* **19**(13), 2918 (2019)
26. Zhang, K., Zuo, W., Chen, Y., Meng, D., Zhang, L.: Beyond a gaussian denoiser: residual learning of deep CNN for image denoising. *IEEE Trans. Image Process.* **26**(7), 3142–3155 (2017)
27. Zhang, X., et al.: Denoising of 3d magnetic resonance images by using higher-order singular value decomposition. *Med. Image Anal.* **19**(1), 75–86 (2015)